Scientia Iranica (2024) 31(4), 310–329

Sharif University of Technology
Scientia Iranica
Transactions B: Mechanical Engineering
https://scientiairanica.sharif.edu

Delamination localization in the composite thin plates using ensemble learning: Bagging and boosting techniques

O. Das[a,*] and D.B. Das[b]

a. *Department of Aeronautics Sciences, Air NCO Higher Vocational School, National Defence University, Gaziemir, Izmir, Türkiye.*
b. *Department of Computer Programming, Ege University, Bornova, Izmir, Türkiye.*

Received 24 September 2021; received in revised form 6 December 2022; accepted 5 April 2023

KEYWORDS
Delamination localization;
Composite structures;
Ensemble learning;
Bagging and boosting;
Machine learning.

Abstract. Localization of the delamination is an essential task that is conducted via various approaches, which may require time, experts, and cost. Various intelligent non-destructive techniques are utilized to reduce time consumption, the need for expertise, and expenditures. Yet, developing an accurate, robust, and low-cost intelligent delamination identification technique becomes a challenging task due to the anisotropy and the variation in the fiber orientation of the composites. Based on those issues, it is aimed to develop an effective intelligent model to localize delaminations in composite plates. This study measures the performance of the Bagging and Boosting techniques on delamination localization in thin composite plates. To validate the effectiveness of the proposed approaches; cross-ply, angle-ply, and quasi-isotropic composite plates having 2400 different delamination cases are considered. The bagging and boosting models are trained with the vibrational characteristics of the healthy and delaminated composite structures. The free vibration analysis is conducted for those structures to obtain the first five natural frequencies and the corresponding mode shapes. For this purpose, classical plate theory is employed by using finite element analysis. It is concluded that bagging and boosting techniques are robust, precise, and accurate in localizing delamination.

1. Introduction

Composite structures are employed in various engineering fields due to their high strength and low weight. However, the phenomenon called delamination may occur due to a lack of reinforcement of fibers through the thickness of the structure [1]. It is essential to check and detect delaminations for reliable and safe to operate composite structures. Nevertheless, performing a destructive or non-destructive test to identify delaminations requires time, experts, and costs. Thanks to advancements in computer science, we can identify delaminations or damages using machine learning techniques based on non-destructive testing methods. Therefore, researchers have developed and

*. *Corresponding author. Tel.: +90 232 311 14 75*
E-mail address: odas@msu.edu.tr (O. Das)

To cite this article:
O. Das, and D.B. Das "Delamination localization in the composite thin plates using ensemble learning: Bagging and boosting techniques", *Scientia Iranica* (2024), **31**(4), pp. 310-329
DOI: 10.24200/sci.2023.59136.6072

utilized various techniques on numerous damage scenarios of different structures [2–18].

Jac Fredo et al. [19] employed composite images to classify damages using Zernike moments and Support Vector Machines (SVMs). They concluded that the features of Zernike moments give better prediction accuracy when compared to the geometrical properties. Inkoom et al. [20] investigated the pavement crack rating using various machine-learning methods. They found that K-nearest neighbor shows the best performance. Gomes et al. [21] employed the reduced mode shapes with Genetic Algorithm (GA) and Artificial Neural Networks (ANNs) to perform delamination identification on the laminated composite plates. They concluded that GA and ANNs are effective in both localizing and identifying the severity of delamination. Zhang et al. [22] studied vibration-based delamination detection in curved composite plate structures using ANNs and Surrogate Assisted Genetic Algorithm (SAGA). They found that ANNs and SAGA models predicted the delamination with 89% and 90.54% accuracy, respectively. He et al. [23] compared various machine learning algorithms for delamination detection in laminated composite beams. They considered natural frequency shifts for model training and testing. They concluded that the SVMs are practically the best model among the three models that they investigated. Jacobs et al. [24] studied the vibrational detection of delamination in composite structures by employing Random Forest (RF) regression. They employed six natural frequencies to predict the location and area of 400 delaminations. Gillespie et al. [25] used transient thermal conduction profiles for delamination detection using support vector classification. They evaluated an F_1 score with 99% accuracy.

Jaanuska and Hein [26] employed Haar Wavelets to identify delamination by using ANNs and RF. Their analysis results indicated that using RF has better performance in identifying delaminations if the problem is approached as a regression problem while ANNs is superior if the problem is taken as a classification problem. Li et al. [27] used ANNs and RF to predict the delamination of the laminated plate. They employed Principal Component Analysis (PCA) to improve the prediction accuracy that is adversely affected by the noise. They concluded that employing PCA causes a decrease of 10% in error rate under noise up to 10% of the input signals. Reis et al. [28] used ANNs to detect delamination in composite beams. For this purpose, they employed vibration responses to feed the ANNs for delamination detection. They concluded that when compared to traditional vibration-based delamination identification techniques, using ANNs significantly drops the computational cost and detects the delamination effectively. Mardanshahi et al. [29] utilized Lamb wave propagation to propose a non-destructive method to detect matrix cracking in cross-ply laminated composites. They predicted the matrix cracking by comparing the elastic modulus and viscoelastic properties obtained through inverse Lamb wave propagation. Their analysis results indicated that the proposed method is in good agreement with the Hashin model. Zheng et al. [30] proposed a two-step technique experience-based learning algorithm to identify delamination in composite beams. They used one-dimensional equivalent through-thickness beam elements to model the composite beam and to identify the potential delamination locations. Moorthy and Marappan [31] identified the delamination severity in tapered fiber-reinforced polymer laminated composite plates by using the Surrogate-Assisted Real-coded Genetic Algorithm (SARGA) and ANNs. The analysis results indicated that although SARGA and ANNs give good prediction results for the numerical data, ANNs fail to predict delamination regarding experimental results. Xu et al. [32] employed a full-scale promoted Convolutional Neural Network (CNN) based 3D Terahertz non-destructive technique to identify delaminations in glass-fiber-reinforced polymer composites. According to the analysis results, they validated the effectiveness of the proposed approach in the localization and imaging of delaminations. Rautela et al. [33] used two approaches to identify delaminations in composite plates. They employed PCA, Independent Component Analysis (ICA), and one-class SVM. Besides, deep learning-based Convolutional Auto-Encoders (CAE) are employed. They concluded that CAE gives better results when compared with the other approach. Mardanshahi et al. [34] employed Guided Wave Propagation (GWP) and ANNs to detect and classify matrix cracking in laminated composites. They also employed Linear Discriminant Analysis (LDA) to find the linear combination of features for better classification. Besides, they used SVMs, Linear Vector Quantization (LVQ), and Multi-Layer Perceptron (MLP) for classification. Among the utilized machine learning techniques, they concluded that SVM gives the best results with an accuracy of 91.7% when compared with others. Barman et al. [35] used Mixed Unified Particle Swarm Optimization (MUPSO) to identify delaminations in composite beams and plates. They used vibration responses of those structures to obtain the rough locations of damages from a mode shape curvature-based damage index. They concluded that the proposed approach is effective and shows good potential in the corresponding field. Lim et al. [36] employed RF to detect delaminations in composite plates. They used the first four natural frequency shifts to detect the delaminations by using RF. They concluded that the proposed approach is effective since it predicts the delaminations with an average coefficient of correlations of 0.98.

Table 1. Comparison of the present study with the existing literature by various aspects considering bagging (RF), boosting AB-RT, and other (ANNs, SVMs, etc. - Oth).

Study	Delamination locations	Localization regions	Fiber orientation	Input parameters	Problem approach	RF	AB-RT	Oth
[23]	657	-One axis -Interface	-Symmetric -Cross-ply	First six natural frequencies	Regression classification			+
[24]	4	-One axis -Interface	-Symmetric -Cross-ply	First six natural frequencies	Regression	+		
[18]	12	-One axis -Interface	-Symmetric -Cross-ply	Transient responses	Classification	+		+
[22]	150	-Two axis -Interface	-Symmetric	First five natural frequency shifts	Regression			+
Present study	800	-Two axis -Interface	-Symmetric -Cross-ply -Angle-ply -Quasi-isotropic	First five natural frequency shifts, slope shifts of the mode shapes	Classification	+	+	

The Ensemble Learning techniques combine the classifiers to come up with an accurate and robust model to solve a particular problem. By doing so, the performance of the classifier is improved. Therefore, it can be concluded that employing Ensemble Learning techniques may be useful for many engineering applications. Due to such positive aspects, we employed two Ensemble Learning techniques namely, Bagging and Boosting to solve the localization of the delaminations. Table 1 presents detailed comparative literature studies that cover delamination localization. It is seen that although there are numerous studies on delamination localization, the performance of these techniques on the localization of delaminations in two-axis and interfaces using ensemble learning techniques has not been measured yet. Besides, the effects of fiber orientation on the input variables and on the performance metrics of these models have not been examined. This study fills this gap by measuring the ability of the bagging and boosting techniques on the localization of the delaminations of cross-ply, angle-ply, and quasi-isotropic cantilever composite plates. For this purpose, we employed the classical plate theory and performed finite element analysis to model the healthy and delaminated structures. Afterward, the first five natural frequency shifts and the slope shifts of the corresponding mode shapes have been evaluated for a total of 2400 delamination cases. The obtained data has been used for model training and testing the Ensemble Learning techniques. To ensure the validity of the machine learning model, the k-fold cross-validation method has been employed.

The contributions of this study are presented as follows:

(i) Measuring the classification performance of Bagging and Boosting Ensemble Learning techniques on the localization of delaminations in two-axis and interfaces for the first time;

(ii) Examining the effects of the different fiber orientations on the selection of input variables to train the machine learning models for the first time;

(iii) Measuring the effects of the various fiber orientations on the classification performance of the machine learning models for the first time.

2. Mathematical modelling

2.1. Finite element analysis of the healthy structures

A four-node quadrilateral element with a total of 20 degrees of freedom has been employed to obtain the mathematical model of the cantilever thin composite plates shown in Figure 1.

To perform the finite element free vibration analysis, it is necessary to accurately express the stress-strain

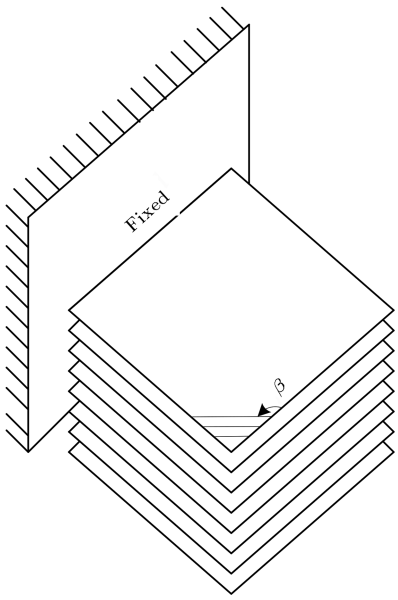

Figure 1. A cantilever composite plate structure.

relation of the thin structure. Therefore, the classical plate theory has been considered. The displacement functions based on this theory are given as [37]:

$$u(x,y,z) = u_0 + z\frac{\delta w}{\delta y}, \qquad \theta_x = \frac{\delta w}{\delta y},$$

$$v(x,y,z) = v_0 + z\frac{\delta w}{\delta x}, \qquad \theta_y = -\frac{\delta w}{\delta x},$$

$$w(x,y,z) = w_0, \tag{1}$$

where u and v are the in-plane displacements, w, θ_x and θ_y represent the out-of-plane displacements. The displacement equations can be written in terms of the shape functions of a four-node quadrilateral element as:

$$u = \sum_{i=1}^{4} u_i N_{li}, \qquad v = \sum_{i=1}^{4} v_i N_{li}, \qquad w = \sum_{i=1}^{4} w_i N_{bi}, \tag{2}$$

where N_{li} and N_{bi} represent the shape functions of the ith node of the finite element [37].

According to the classical plate theory, the stress-strain relations can be expressed as [37]:

$$\{\sigma\} = [D_m]\{\epsilon\}, \tag{3}$$

where $\{\sigma\}$ denotes the stress matrix including in-plane and out-of-plane resultants. $\{\epsilon\}$ is the strain matrix and $[D_m]$ is the material stiffness matrix, which can be written as [37]:

$$[D_m] = \begin{bmatrix} \mathbf{A} & \mathbf{B} \\ \mathbf{B} & \mathbf{C} \end{bmatrix}, \tag{4}$$

where $\boldsymbol{A}$, $\boldsymbol{B}$, and $\boldsymbol{C}$ represent the longitudinal, longitudinal-bending coupled, and bending stiffness components. Therefore:

$$\mathbf{A} = \sum_{k=1}^{NL} [F_{ij}]^k (z_k - z_{k-1}),$$

$$\mathbf{B} = \frac{1}{2}\sum_{k=1}^{NL} [F_{ij}]^k (z_k^2 - z_{k-1}^2),$$

$$\mathbf{C} = \frac{1}{3}\sum_{k=1}^{NL} [F_{ij}]^k (z_k^3 - z_{k-1}^3), \tag{5}$$

where NL is the number of layers and $[F_{ij}]^k$ $(i,j = 1,2,6)$ is the material constants matrix of the kth layer of the structure based on the fiber angle. Therefore:

$$[F]^k = [H]^T \begin{bmatrix} [F'_{11}] & [F'_{12}] & 0 \\ [F'_{21}] & [F'_{22}] & 0 \\ 0 & 0 & [F'_{66}] \end{bmatrix} [H], \tag{6}$$

and:

$$[F'_{11}] = \frac{E_x}{1-\nu_{xy}\nu_{yx}}, \qquad [F'_{12}] = \nu_{yx}[F'_{11}],$$

$$[F'_{21}] = [F'_{12}], \qquad [F'_{22}] = \frac{E_y}{1-\nu_{xy}\nu_{yx}},$$

$$[F'_{66}] = G_{xy}, \tag{7}$$

where E_x and E_y are the young modulus of the material in the x- and y-axis. G_{xy} is the shear modulus with respect to x- and y-direction, ν_{xy} and ν_{yx} are the Poisson's ratio in the xy- and yx- direction [37]. H is the transformation matrix, which is:

$$[H] = \begin{bmatrix} \cos^2\beta & \sin^2\beta & \frac{1}{2}\sin 2\beta \\ \sin^2\beta & \cos^2\beta & -\frac{1}{2}\sin 2\beta \\ -\sin 2\beta & \sin 2\beta & \cos 2\beta \end{bmatrix}, \tag{8}$$

where β is the fiber angle. The element strain energy (U) can be evaluated as [37]:

$$U = \frac{1}{2}\int_{-1}^{1}\int_{-1}^{1} \{\delta\}^T [B_{ls}]^T [D_m][B_{ls}]\{\delta\}|J|d\xi d\eta, \tag{9}$$

where $|J|$ represent the determinant of the Jacobian matrix and:

$$[B_{ls}] = \sum_{i=1}^{4} \begin{bmatrix} \frac{\delta N_{li}}{\delta x} & 0 & [0]_{1x3} \\ 0 & \frac{\delta N_{li}}{\delta y} & [0]_{1x3} \\ \frac{\delta N_{li}}{\delta y} & \frac{\delta N_{li}}{\delta x} & [0]_{1x3} \\ 0 & 0 & [\frac{\delta^2 N_{bi}}{\delta x^2}]_{1x3} \\ 0 & 0 & [\frac{\delta^2 N_{bi}}{\delta y^2}]_{1x3} \\ 0 & 0 & [\frac{\delta^2 N_{bi}}{\delta xy}]_{1x3} \end{bmatrix} \tag{10}$$

where:

$$\{\delta\}^T = \{u_i \;\; v_i \;\; w_i \;\; \theta x_i \;\; \theta y_i\}. \tag{11}$$

The element kinetic energy (T) can be calculated as [37]:

$$T = \frac{1}{2}\int_{-1}^{1}\int_{-1}^{1}\{\delta\}^T[N_a]^T[Q][N_a]\{\delta\}|J|d\xi d\eta, \quad (12)$$

where:

$$[N] = \sum_{i=1}^{4}\begin{bmatrix} N_{li} & 0 & 0 & 0 & 0 \\ 0 & N_{li} & 0 & 0 & 0 \\ 0 & 0 & N_{li} & 0 & 0 \\ 0 & 0 & 0 & N_{bi} & 0 \\ 0 & 0 & 0 & 0 & N_{bi} \end{bmatrix}, \quad (13)$$

and:

$$[Q] = \begin{bmatrix} t\rho & 0 & 0 & 0 & 0 \\ 0 & t\rho & 0 & 0 & 0 \\ 0 & 0 & t\rho & 0 & 0 \\ 0 & 0 & 0 & I\rho & 0 \\ 0 & 0 & 0 & 0 & I\rho \end{bmatrix}, \quad (14)$$

where ρ denotes the density of the material, t is the thickness of the element, and I represents the moment of inertia. Hence, the element strain and kinetic energy equations can be written in the matrix form as [37]:

$$U = \frac{1}{2}\int_{-1}^{1}\int_{-1}^{1}\{\delta\}^T[k_{el}]\{\delta\}|J|d\xi d\eta, \quad (15)$$

$$T_e = \frac{1}{2}\int_{-1}^{1}\int_{-1}^{1}\{\delta\}^T[m_{el}]\{\delta\}|J|d\xi d\eta, \quad (16)$$

where $[k_{el}]$ and $[m_{el}]$ are the element stiffness and mass matrices, respectively. For a conservative system, the equation of motion can be expressed through Lagrange equations as:

$$[M]\{\ddot{\delta}\} + [K]\{\delta\} = 0, \quad (17)$$

where $[K]$ and $[M]$ are the global stiffness and mass matrices. The equation of motion can be represented by an eigenvalue problem to calculate the natural frequencies of the structure. Hence, the eigenvalue problem for the free vibration analysis is:

$$([K] - \omega^2[M]) = 0, \quad (18)$$

where ω represents the natural frequency values of the structure and the corresponding eigenvectors are the displacement values of the relevant mode shapes of the structure.

2.2. Finite element analysis of the delaminated structures

Figure 2 shows the healthy (A), lower (B), and upper (C) sections of an illustrative plate structure. The finite element model of the delaminated composite plate has been obtained by considering the material stiffness matrices of the lower and upper layers of the delaminated interface [38].

Therefore, the longitudinal, longitudinal-bending coupled, and bending stiffness components, given in Eq. (7) has been calculated for the lower (low) and upper (up) section as:

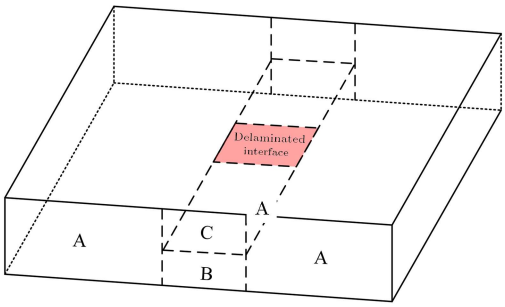

Figure 2. An illustration of a composite plate with a central delamination.

$$[A_{low}] = \sum_{k=1}^{p}[F_{ij}]^k(z_k - z_{k-1}),$$

$$[A_{up}] = \sum_{k=p+1}^{NL}[F_{ij}]^k(z_k - z_{k-1}),$$

$$[B_{low}] = \frac{1}{2}\sum_{k=1}^{p}[F_{ij}]^k(z_k^2 - z_{k-1}^2),$$

$$[B_{up}] = \frac{1}{2}\sum_{k=p+1}^{NL}[F_{ij}]^k(z_k^2 - z_{k-1}^2),$$

$$[C_{low}] = \frac{1}{3}\sum_{k=1}^{p}[F_{ij}]^k(z_k^3 - z_{k-1}^3),$$

$$[C_{up}] = \frac{1}{3}\sum_{k=p+1}^{NL}[F_{ij}]^k(z_k^3 - z_{k-1}^3), \quad (19)$$

where p is the number of upper and lower layers. Hence, the material stiffness matrix of the delaminated section can be evaluated by simply summing the stiffness components of the upper and lower sections. The remained procedure is the same as given in Section 2.1.

3. Material and method

3.1. Convergence analysis

In this study, delamination detection on the various cantilever composite plates has been performed using bagging and boosting techniques. For this purpose, the cantilever graphite/epoxy composite plate structures have been mathematically modeled using the finite element method. Three stacking sequences have been considered to measure the effects of fiber orientation on prediction performance. Therefore a cross-ply $[90^0/0^0]_{2s}$, an angle-ply $[60^0, -60^0]_{2s}$, and a quasi-isotropic $[0^0/90^0/45^0/-45^0]_s$ fiber orientation has been

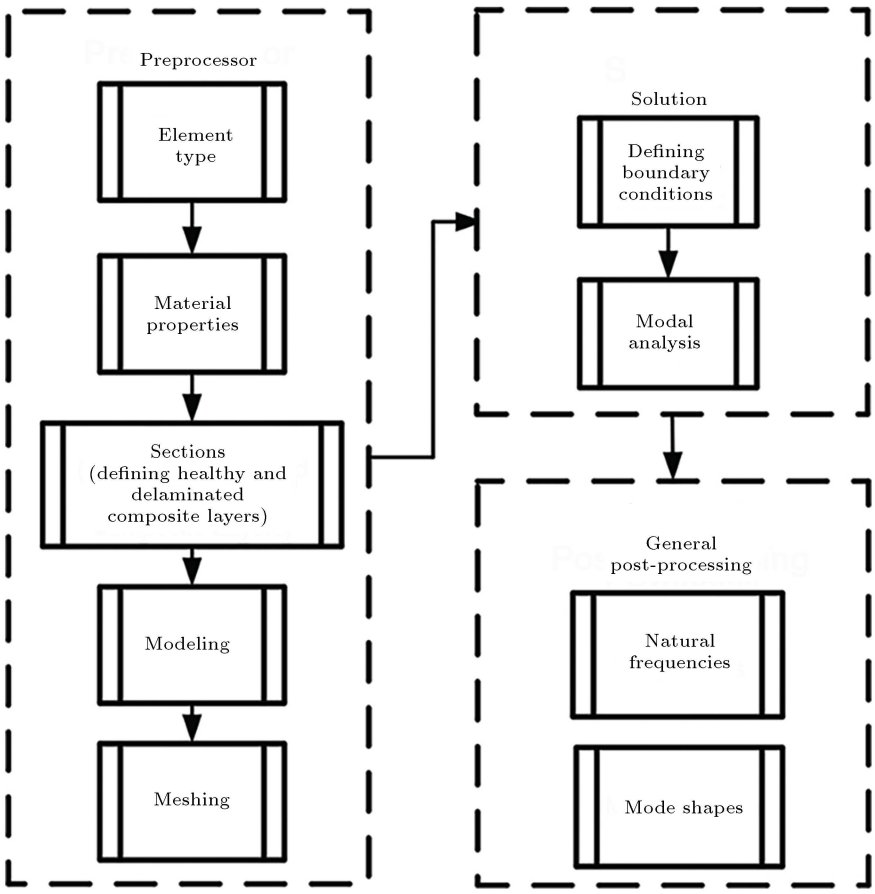

Figure 3. The flowchart of the convergence analysis conducted in ANSYS.

taken into account. To verify the correctness of the analytical approach given in Section 2, a convergence analysis is performed via numerical analysis conducted in ANSYS 18.2. Figure 3 shows the flowchart of the procedure conducted for convergence analysis within ANSYS.

Table 2 gives the mechanical and geometrical properties of the composite plates [39]. The mathematical model of the structures has been verified by comparing the results of the free vibration analysis of both healthy and delaminated quasi-isotropic cantilever composite plates by using ANSYS 18.2. The quasi-isotropic orientation, has been chosen since it can show whether the mathematical model gives accurate results regardless of the fiber angle. The finite element model of the structure has been developed in ANSYS by assembling 100 mm-sized SHELL181 elements. In total, the ANSYS model comprises 100 elements and 121 nodes as shown in Figure 4. Each layer is constructed using Shell Sections where the values of the fiber angle and the thickness of the layer have been provided. To introduce delamination, the delaminated interface has been defined considering the mechanical properties of air. The remained healthy layers have been defined just as they are provided for healthy structures. Table 3 shows the convergence analysis results of the healthy and delaminated quasi-isotropic cantilever composite plate structure. It is seen that the considered mathematical model is in good agreement

Table 2. The material and geometrical properties of the composite plate structure.

Material and geometrical properties	
E_x (GPa)	206.8
E_y (GPa)	5.17
E_z (GPa)	5.17
G_{xy} (GPa)	2.55
G_{xz} (GPa)	2.55
G_{yz} (GPa)	1.38
ρ (kg/m^3)	1528
$\nu_{xy} = \nu_{xz} = \nu_{yz}$	0.25
Length (mm)	1000
Width (mm)	1000
Layer thickness (mm)	1.25
Number of layers	8

Table 3. Convergence analysis results of healthy and delaminated cantilever quasi-isotropic composite structures.

Healthy				Delaminated			
Mode	Analytical results (present study) (Hz)	Numerical results (ansys) (Hz)	Difference (Hz)	Mode	Analytical results (present study) (Hz)	Numerical results (ansys) (Hz)	Difference (Hz)
1	5.892	5.905	0.013	1	5.892	5.893	0.001
2	8.617	8.632	0.015	2	8.606	8.650	0.044
3	30.910	31.159	0.249	3	30.893	31.053	0.160
4	37.217	37.639	0.422	4	37.207	37.179	0.028
5	41.086	41.448	0.362	5	41.071	41.088	0.017
6	57.875	58.188	0.313	6	57.849	57.780	0.069
7	80.993	82.713	1.720	7	80.989	80.826	0.163
8	100.160	101.440	1.280	8	100.120	99.897	0.223
9	106.100	108.730	2.630	9	106.090	105.430	0.660
10	109.480	111.910	2.430	10	109.460	108.840	0.620

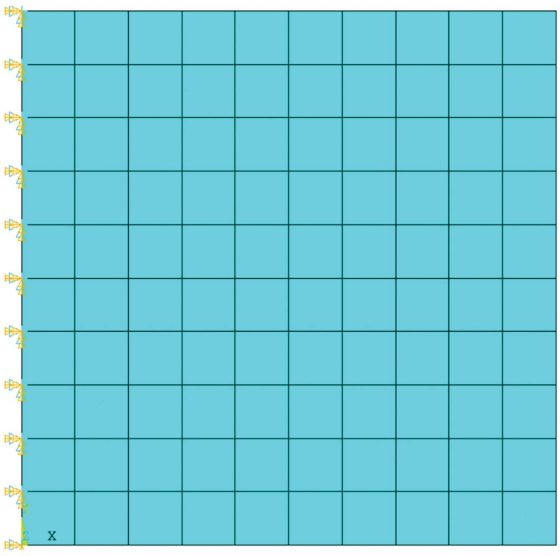

Figure 4. Composite plate structure meshed in ANSYS.

with those of ANSYS for both healthy and delaminated structures.

3.2. Machine learning approaches

The experimental analyses have been performed by using two Ensemble Learning techniques namely, Bagging (RF) and Boosting (AB-RT) to predict the delamination located in the close-to-edge and center layers throughout the cantilever plate structure. The experiments have been conducted for each Ensemble Learning technique, plate structure, and location outputs, which are the interface region, x-axis region on the surface, and y-axis region on the surface. Figure 5 shows an illustration of the considered delamination location parameters. According to Figure 5, the delamination is located in the second interface and the first finite element of the structure. This location information has been expressed as the delamination that existed in the close-to-edge interfaces and the intersection of A_x and A_y regions. Therefore, a total of 18 experiments have been performed. Figure 6 shows the brief flowchart of the study.

The input parameters have been chosen as the first five natural frequency shifts and the slope shifts of the corresponding mode shapes in the perspective of the xz- and yz-planes. To validate the model, the 10-fold cross-validation method has been employed. Each experiment has been conducted after tuning the number of iterations required to obtain the best model that localizes the delamination. Therefore, all experiments have been conducted by considering 10 iterations for AdaBoost-Random Tree (AB-RT). On the other hand, the optimal number of iterations is obtained as 100 for RF for both localizing the delamination within the x-axis and y-axis regions, while it is evaluated as 10 for interface-based localization experiments. To interpret the results and measure the validity of the machine learning model, performance metrics such as classification accuracy, F-measure, AUC value, kappa score, and confusion matrix have been considered.

3.3. Bagging (RF)

The main goal of RF is to lower the variance by averaging the results and obtaining a community that comprises low-correlated Random Trees [40]. The evaluation of those trees is performed by randomization. This process requires two steps. The first step is growing the trees by conducting observations of randomly chosen sub-dataset. In the second step, the nodes of each tree are split by employing input variables of the chosen sub-dataset. Afterward, these trees

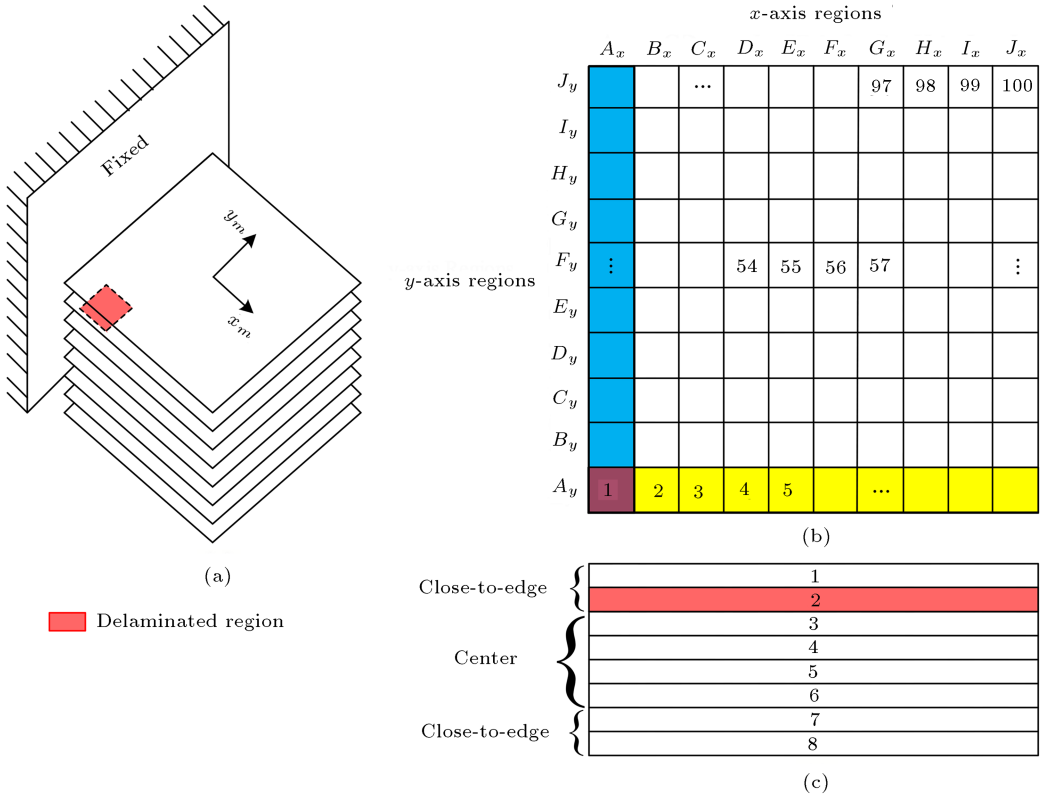

Figure 5. (a) Isometric view of a delaminated plate including location parameters in terms of, (b) x-axis and y-axis regions and (c) interface.

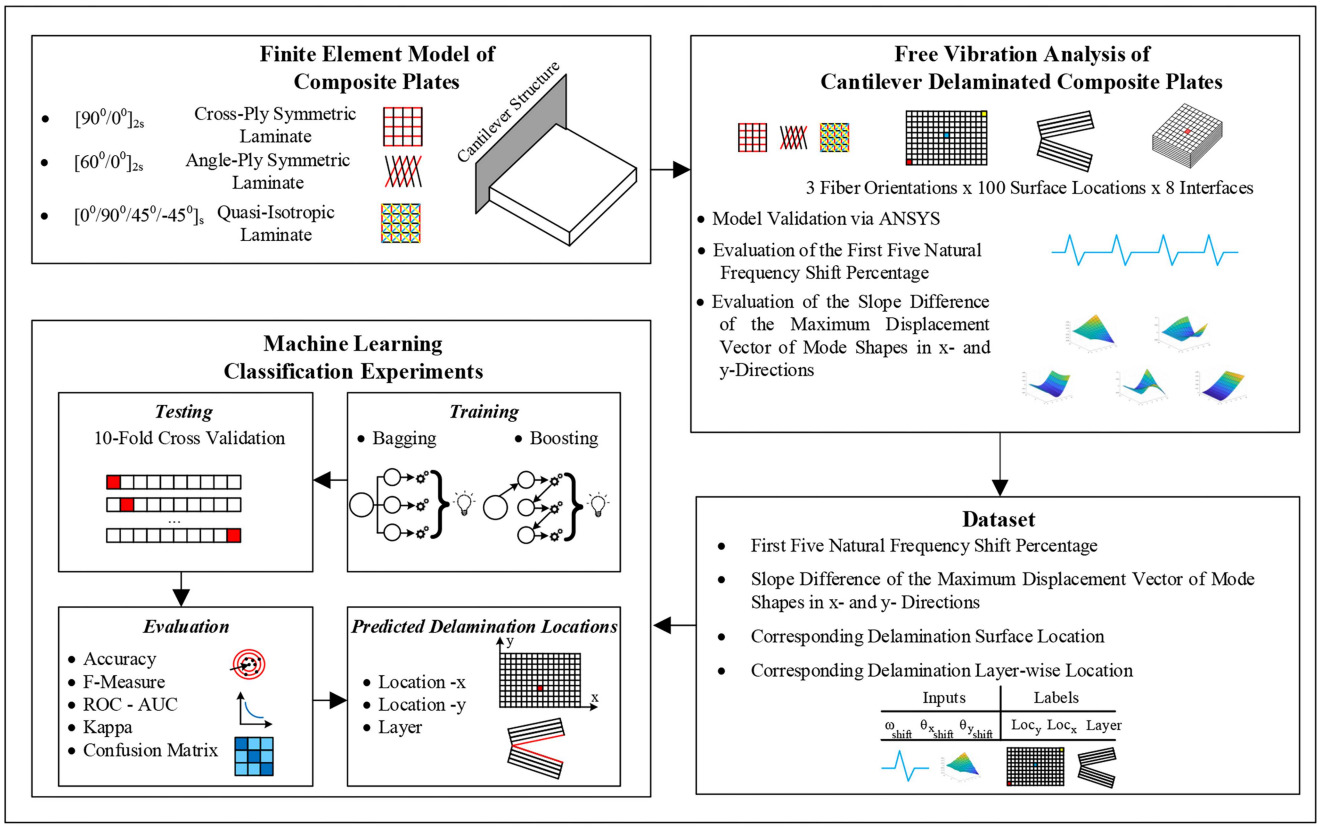

Figure 6. The flowchart of the study.

are associated to obtain RF. The brief mathematical expression of the RF is:

$$Y(x) = \frac{1}{B_n}\sum_{i=1}^{B_n} y_i(x) + e, \tag{20}$$

where $Y(x)$ is the new prediction for each new observation (x), B_n denotes the number of bagging processes, $y_i(x)$ is the calculated prediction by using each Random Tree, and e represents the error.

3.4. Boosting (AB-RT)

AdaBoost or Adaptive Boosting aims to develop an accurate prediction model by associating moderately inaccurate and rough rules [41].

The boosting process can be summarized as generating a final rule after C_s round by the combining of weak hypotheses of each distribution, which is built by the booster on each cycle, $c = 1, 2, ..., C_s$. By boosting the process, AdaBoost increases the prediction accuracy of the weak classifier. RF is constituted of Random Trees as the base learner. Using trees have a low computational cost in prediction. They are also able to handle both categorical and numerical data and give accurate results even in a presence of a problem in some parts of the data. Due to those positive aspects, trees are advantageous. Using those trees as the base learner for bagging or boosting techniques increases their positive aspects to a higher level. Since RF is constituted by those trees, we also considered Random Trees for the AdaBoost algorithm to make a homogeneous comparison with RF. The mathematical expressions of AdaBoost are briefly given as:

$$B_{C_s} = \sum_{c=1}^{C_s} b_c(x),$$

$$err_{C_s} = \sum_{k} err[F_{c-1}(x_k) + \zeta_c hyp(x_k)], \tag{21}$$

where B_{C_s} denotes the boosted classifier while b_c is a weak learner, which considers x as inputs and returns an outcome that represents the class. For each sample that existed in the training dataset, the weak learner gives a hypothesis, $hyp(x)$. In this study, the Random Tree has been considered as the base learner. It can be seen from Eq. (24) that the final error value of the boosted classifier is evaluated by the summation of the error of the previously boosted classifier F_{c-1} and the multiplication of the produced hypothesis by a selected coefficient ζ_c. This process is performed until the sum of the final error of the boosted classifier err_{C_s} is minimized.

3.5. Dataset

The dataset obtained within this study includes 800 delamination scenarios for each cantilever composite plate structure. Since cross-ply, angle-ply, and quasi-isotropic plates have been considered, the dataset comprises a total of 2400 instances and 18 attributes. These attributes are the first five natural frequency shifts and the slope shifts of the corresponding mode shape in the perspective of the xz-, and yz-planes. The first five natural frequency shifts and the slope differences of the corresponding mode shapes are considered as the input parameters while the delamination locations, which are close-to-edge or center interfaces and two-axis surface-wise location of the delamination have been considered as output parameters. The natural frequency shifts have been evaluated by:

$$\omega_{shift} = 100\frac{\omega_{i_h} - \omega_{i_d}}{\omega_{i_h}}, \tag{22}$$

where ω_{i_h} and ω_{i_d} are the ith natural frequencies of the healthy and delaminated structures, respectively. The slope differences of the maximum displacement vectors have been calculated by:

$$\gamma_{shift_x} = 100\frac{\gamma_{xi_h} - \gamma_{xi_d}}{\gamma_{xi_h}},$$

$$\gamma_{shift_y} = 100\frac{\gamma_{yi_h} - \gamma_{yi_d}}{\gamma_{yi_h}}, \tag{23}$$

where γ_{xi} and γ_{yi} are the slopes of the mode shapes in the perspective of xz- and yz-planes of the ith mode. The subscripts h and d represent the "*healthy*" and "*delaminated*" structures, respectively. Figure 7 shows an illustration of the perspectives of the second mode shape of the cantilever quasi-isotropic composite structure in xz- and yz-planes.

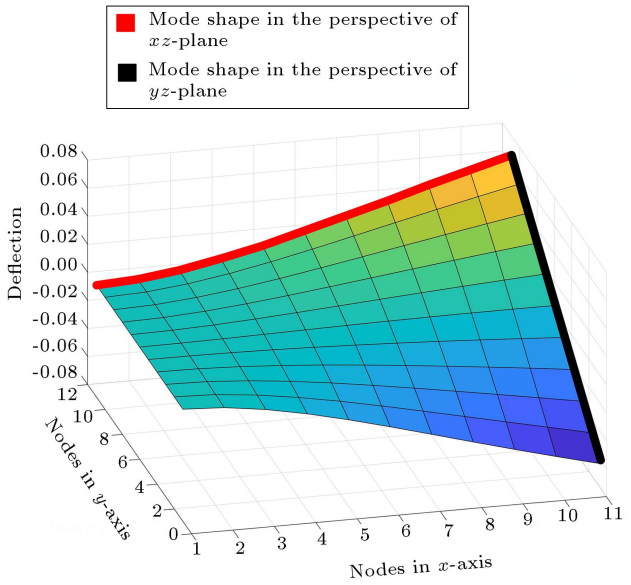

Figure 7. The perspectives in xz- and yz- planes of the second mode shape of the cantilever quasi-isotropic composite structure.

4. Results and discussion

The experiments have been conducted using the first five natural frequency shifts and slope shifts of the mode shapes in the perspectives of the xz- and yz-planes. For each location, the first five natural frequency shifts have been calculated and plotted. Figures 8–10 show the effect of the location of delamination considering x-axis regions, y-axis regions, and interfaces.

It is seen from Figure 8 that the natural frequency shifts fluctuate as the delamination location changes along the F_x region. On the other hand, Figure 9 indicates that as the delamination location changes along the F_y region, the natural frequency shifts of the cross-ply structure vary symmetrically, while those of the angle-ply and quasi-isotropic structure differ uniquely without indicating any symmetrical pattern. This situation causes the model to confuse since the delaminations, which are located symmetrically to the x_m-axis, lower the natural frequencies by the same amount. Therefore, the machine learning model may give inaccurate results. For instance, consider a delamination located in the first element of the cross-ply plate (see Figure 5) regardless of its interface-wise location. If only the natural frequency shifts have been introduced to the machine learning model, it may predict the location of the delamination in the 91^{st} element, which is symmetric of the first element or actual element to x_m-axis. There are two reasons behind this situation. The first reason is the inclination of the material axes due to the fiber orientation, which distinguishes the other fiber orientations from the cross-ply orientation. Considering symmetric cross-ply laminate, some of the material stiffness constants will simply equal zero since cos(90) and sin(0) are equal to zero. Mathematically, this situation leads some of the bending stiffness components' values to zero, which resulted in symmetrical bending displacement behavior of the mode shape of the cross-ply structure. The

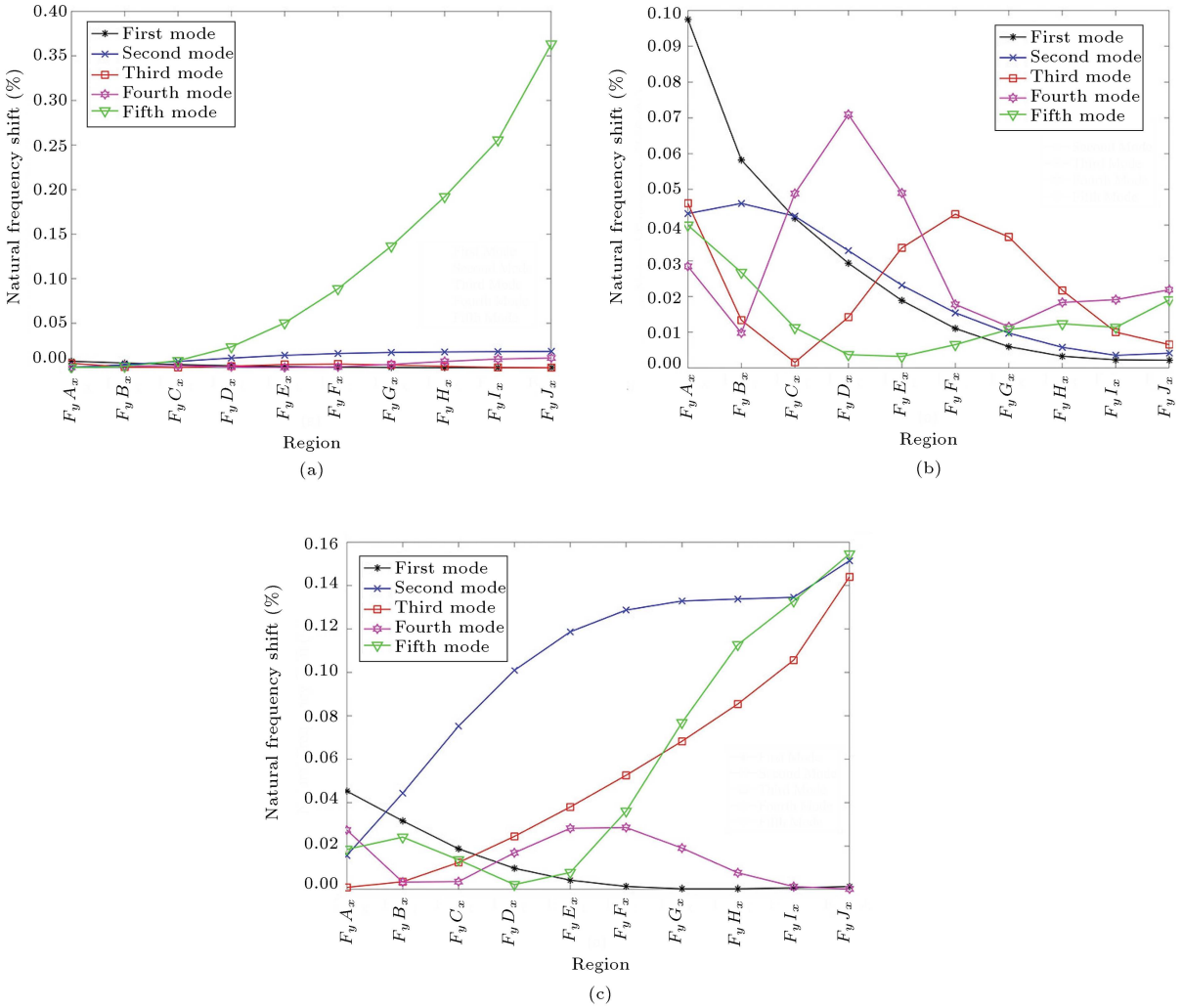

Figure 8. The effect of delamination located in x-axis regions on the first five natural frequencies of the (a) cross-ply, (b) angle-ply, and (c) quasi-isotropic composites.

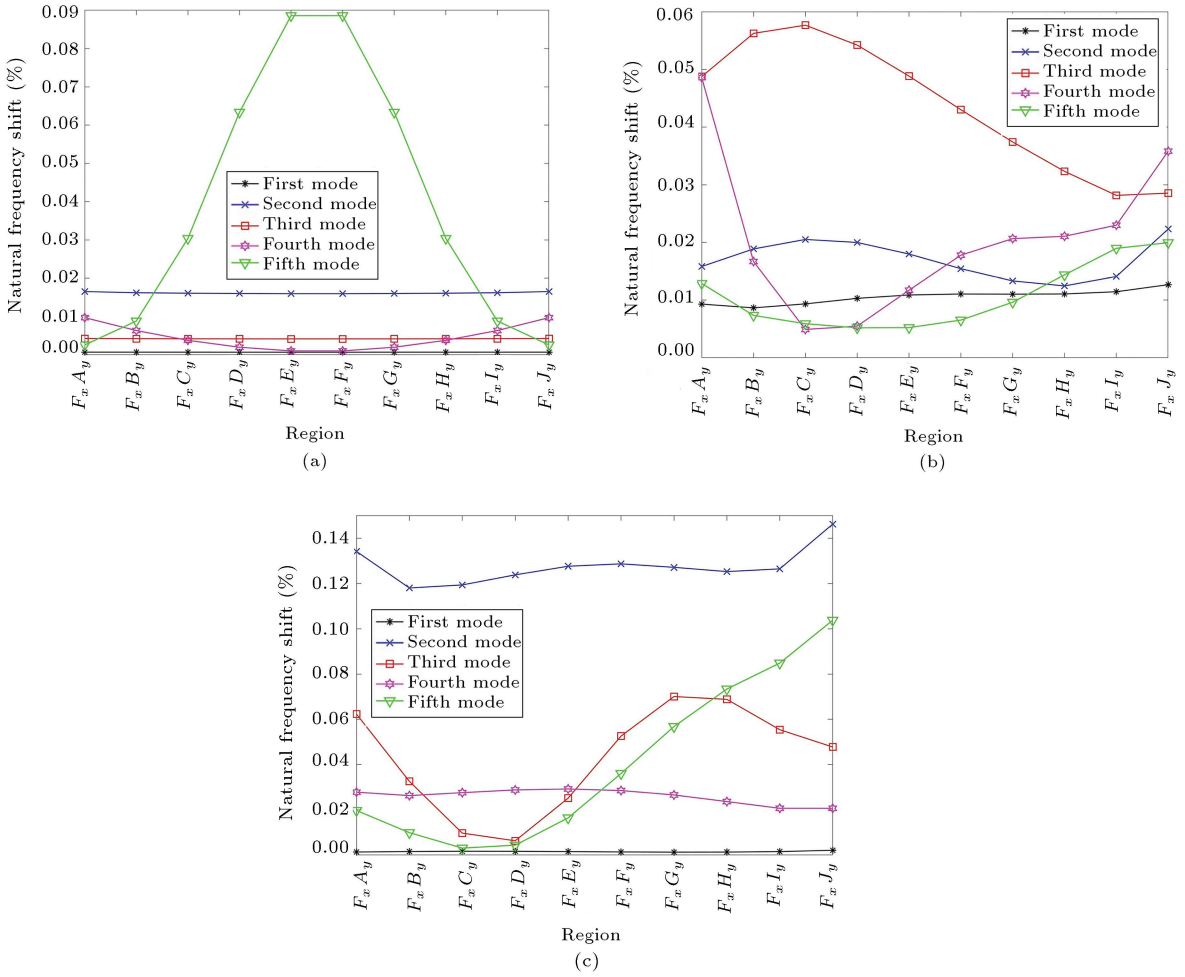

Figure 9. The effect of delamination located in y-axis regions on the first five natural frequencies of the (a) cross-ply, (b) angle-ply, and (c) quasi-isotropic composites.

second reason is the boundary condition. However, this reason is the explanation of why such a phenomenon has taken place by only localizing the delamination in the y-axis. As it is seen from Figure 5, the structure has been fixed from the y-axis. Therefore, the absolute values of the displacements that occurred under and above the x_m-axis are equal while their directions are opposite. To overcome this issue the slope shifts of the mode shapes have been introduced as an additional input variable to the Ensemble Learning techniques.

As seen in Figure 10, the delamination occurrence below and above the neutral axis of the thickness of the structure affects the natural frequencies symmetrically. The reason behind this condition is the absolute values of those displacements are the same no matter which fiber orientation is chosen. Considering the slope shifts as an additional input variable will not make any difference in the prediction performance of the machine learning model since frequency shifts and slope shifts are symmetrical. Therefore, the prediction can be performed by considering the first two and the last two interfaces as the close-to-edge group, and the remained interfaces as the center group of interfaces.

The localization of the delamination procedure is conducted by developing bagging and boosting techniques by using Sklearn, Pandas, and Numpy packages in Python 3.8. Figure 11 shows the flowchart of the delamination localization procedure via bagging and boosting methods. An illustration of the first three depths of a tree built to predict the delamination is shown in Figure 12. Considering the illustration of the partial tree given in Figure 12, the class $y[7]$ (delamination located in the region H_x) is predicted by using the features $X[0]$ (shift of the first natural frequency), $X[4]$ (shift of the fifth natural frequency), and $X[8]$ (slope shift of the x-axis of the second mode shape). A similar procedure is conducted for all trees constituted for the bagging and boosting techniques. The final decision is made for those methods as mentioned in Sections 3.3 and 3.4.

Tables 4–6 and Figures 13–15 give the performance metrics (Acc: Accuracy, F-M: F-Measure, κ: Kappa) and confusion matrices of the RF and AB-RT

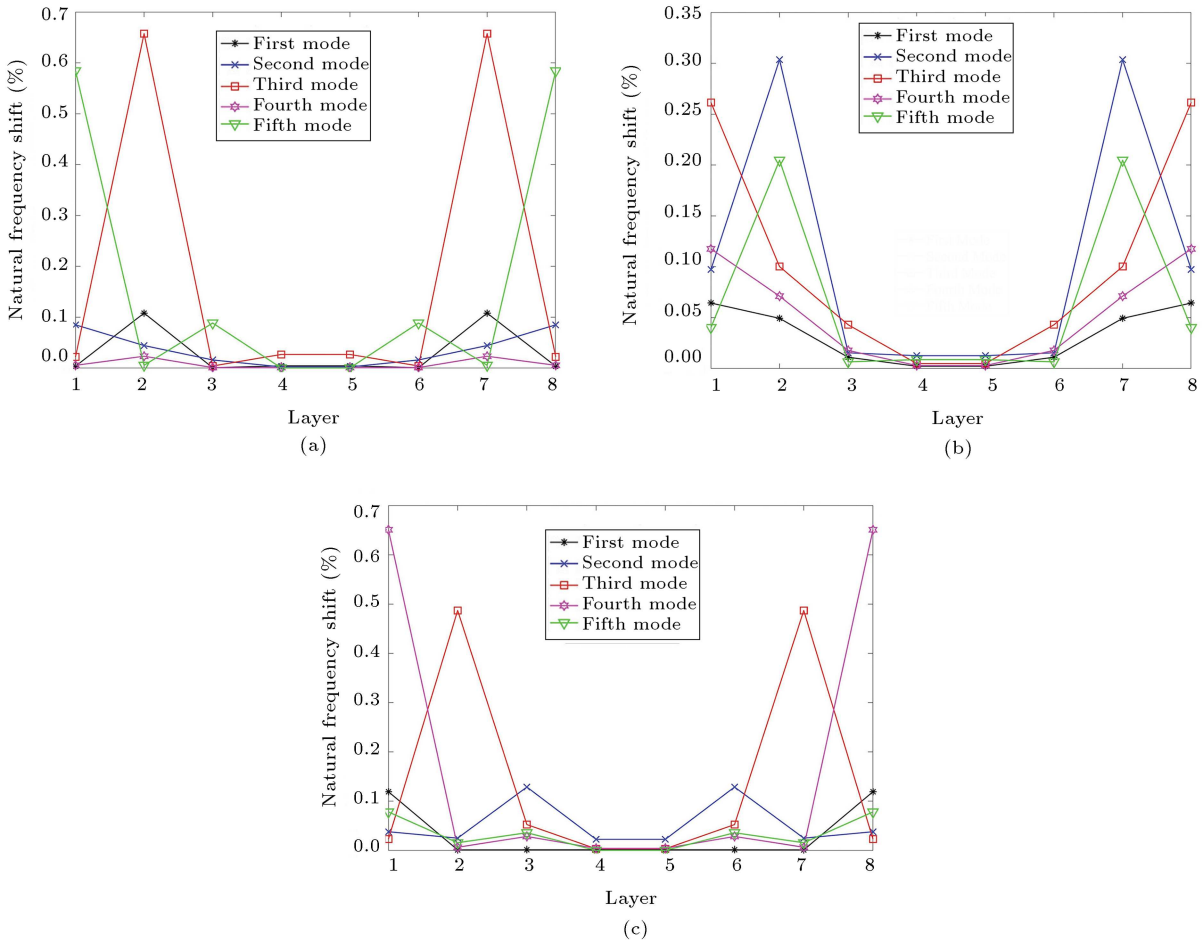

Figure 10. The effect of delamination located in interfaces on the first five natural frequencies of the (a) cross-ply, (b) angle-ply, and (c) quasi-isotropic composites.

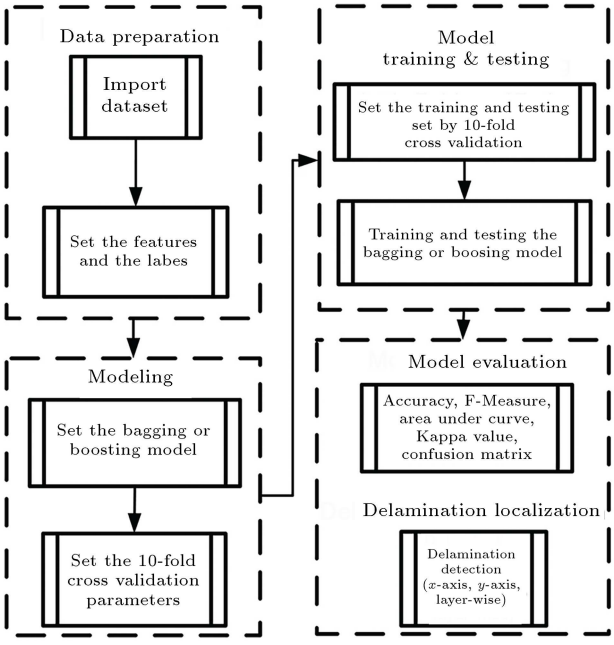

Figure 11. Delamination localization procedure using bagging and boosting techniques.

considering only the first five natural frequency shifts to localize the delamination in the cross-ply, angle-ply, and quasi-isotropic composite cantilever plate structures.

It is seen from Tables 4–6 that, considering only natural frequency shifts as input variables is effective for all cases, except for the localization of delamination in y-regions for the cross-ply composite cantilever plate structure. As it is interpreted for Figure 9, this situation is occurred due to symmetrical variations in the natural frequency shifts. Considering the AUC values, which are 0.854 for AB-RT and 0.927 for RF, it is concluded that the Ensemble Learning models can successfully distinguish the location of the delamination. However, the accuracy, F-Measure, and Kappa values indicate that the prediction performance of the actual location of the delamination is poor.

Regarding the confusion matrix for localization of delamination in y-axis regions shown in Figure 14 it is seen that the machine learning algorithm predicts the delamination as if it is located in the symmetric of its actual location. Because the natural frequency shifts are the same for the symmetric delaminations,

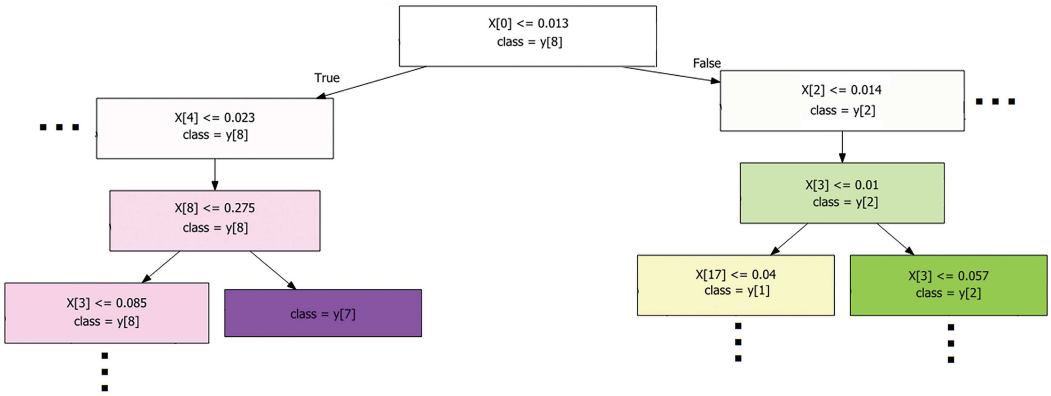

Figure 12. An illustration of the first three depths of a tree.

Table 4. The performance metrics of AB-RT and RF for delamination localization in the x-axis regions of the cross-ply, angle-ply, and quasi-isotropic composite plates considering only the natural frequency shifts.

Cross-ply				Angle-ply				Quasi-isotropic			
AB-RT				AB-RT				AB-RT			
Acc	***F-M***	***AUC***	κ	***Acc***	***F-M***	**AUC**	κ	***Acc***	***F-M***	***AUC***	κ
100%	1.000	1.000	1.000	100%	1.000	1.000	1.000	99.75%	0.998	0.998	0.995
RF				**RF**				**RF**			
Acc	***F-M***	***AUC***	κ	***Acc***	***F-M***	**AUC**	κ	***Acc***	***F-M***	***AUC***	κ
99.75%	0.998	0.998	0.995	99.875%	0.999	1.000	0.998	99.50%	0.995	1.000	0.990

Table 5. The performance metrics of AB-RT and RF for delamination localization in the y-axis regions of the cross-ply, angle-ply, and quasi-isotropic composite plates considering only the natural frequency shifts.

Cross-ply				Angle-ply				Quasi-isotropic			
AB-RT				AB-RT				AB-RT			
Acc	***F-M***	***AUC***	κ	***Acc***	***F-M***	**AUC**	κ	***Acc***	***F-M***	***AUC***	κ
59.00%	0.590	0.854	0.544	94.75%	0.947	0.971	0.942	94.25%	0.942	0.968	0.936
RF				**RF**				**RF**			
Acc	***F-M***	***AUC***	κ	***Acc***	***F-M***	**AUC**	κ	***Acc***	***F-M***	***AUC***	κ
56.63%	0.566	0.927	0.518	93.25%	0.933	0.976	0.925	94.50%	0.945	0.989	0.939

Table 6. The performance metrics of AB-RT and RF for delamination localization in the interfaces regions of the cross-ply, angle-ply, and quasi-isotropic composite plates considering only the natural frequency shifts.

Cross-ply				Angle-ply				Quasi-isotropic			
AB-RT				AB-RT				AB-RT			
Acc	***F-M***	***AUC***	κ	***Acc***	***F-M***	**AUC**	κ	***Acc***	***F-M***	***AUC***	κ
100.00%	1.000	1.000	1.000	100.00%	1.000	1.000	1.000	99.75%	0.998	0.998	0.995
RF				**RF**				**RF**			
Acc	***F-M***	***AUC***	κ	***Acc***	***F-M***	**AUC**	κ	***Acc***	***F-M***	***AUC***	κ
100.00%	1.000	1.000	1.000	99.875%	0.999	1.000	0.998	99.50%	0.995	1.000	0.990

both bagging and boosting methods mispredict the delamination location since they are trained only by the natural frequency shifts. This explains the low accuracy, F-Measure, Kappa values, and high AUC value. It is seen that the models can successfully distinguish the actual delamination location from those that are not symmetric. On the other hand, such a condition has not been observed for other fiber orientations and/or delamination locations as seen in Tables 4–6 and Figures 13–15. It can be interpreted

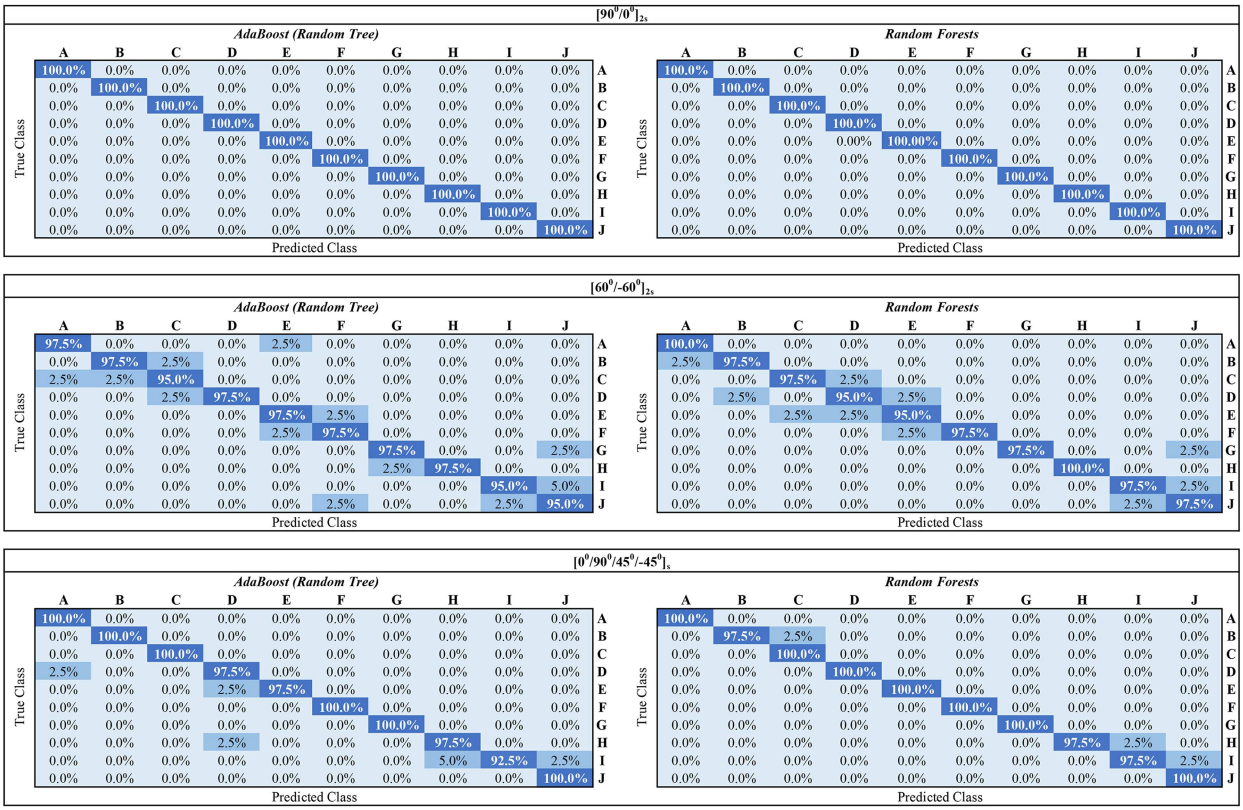

Figure 13. The confusion matrix of AB-RT and RF for delamination detection in x-regions considering only the natural frequency shifts.

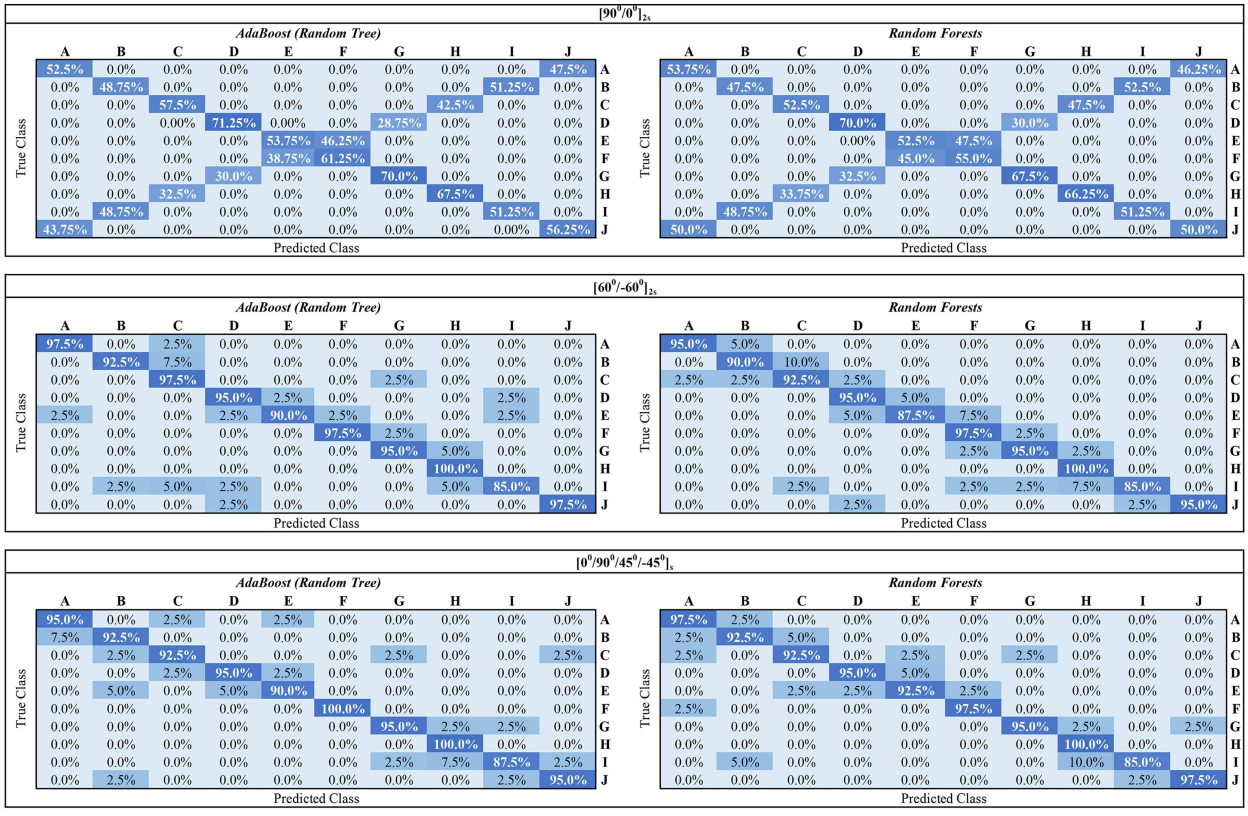

Figure 14. The confusion matrix of AB-RT and RF for delamination detection in y-regions considering only the natural frequency shifts.

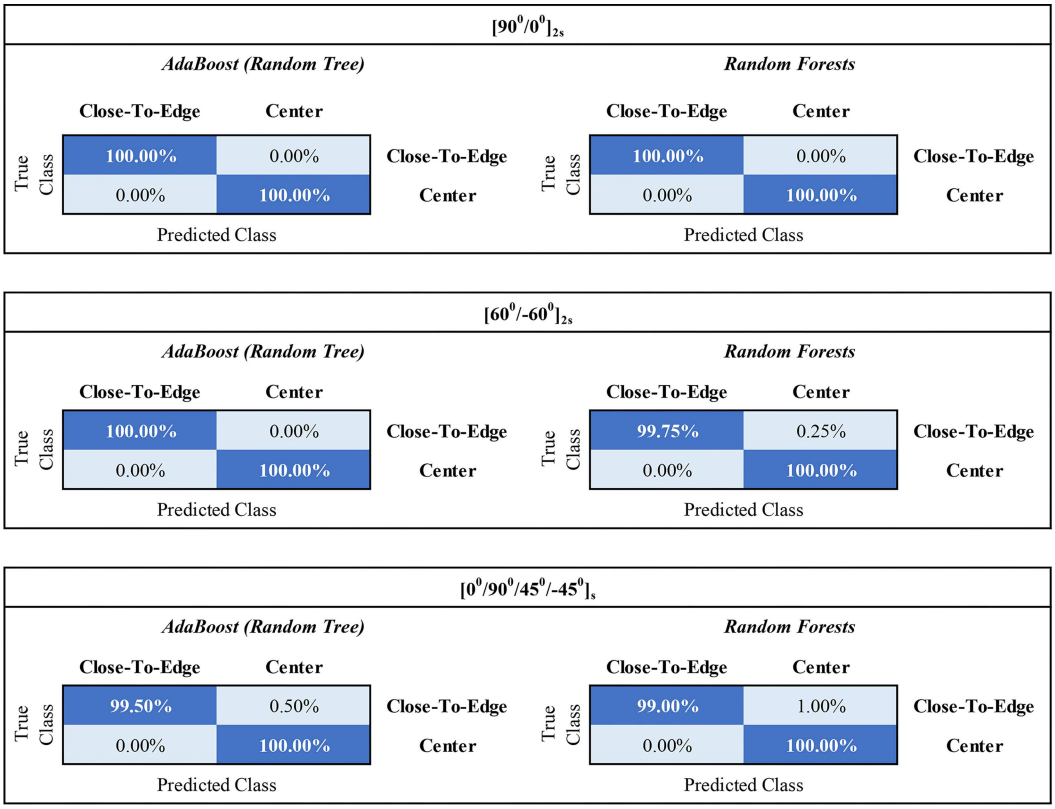

Figure 15. The confusion matrix of AB-RT and RF for delamination detection in interfaces considering only the natural frequency shifts.

Table 7. The performance metrics of AB-RT and RF for delamination localization in the x-axis regions of the cross-ply, angle-ply, and quasi-isotropic composite plates considering both the natural frequency shifts and slope shifts.

Cross-ply				Angle-ply				Quasi-isotropic			
AB-RT				AB-RT				AB-RT			
Acc	*F-M*	*AUC*	κ	*Acc*	*F-M*	AUC	κ	*Acc*	*F-M*	*AUC*	κ
99.75%	0.997	0.999	0.997	97.25%	0.973	0.985	0.969	97.00%	0.970	0.983	0.967
RF				RF				RF			
Acc	*F-M*	*AUC*	κ	*Acc*	*F-M*	AUC	κ	*Acc*	*F-M*	*AUC*	κ
99.88%	0.999	1.000	0.999	98.00%	0.98	1.000	0.978	98.50%	0.985	1.000	0.983

that the localization of delamination in x-axis regions and interface regions has been accurately predicted no matter which fiber orientation has been considered. Besides, for angle-ply and quasi-isotropic structure, localization in y-axis regions has been successfully performed by both RF and AB-RT considering only natural frequency shifts as seen from Tables 4–6 and Figures 13–15. Tables 7–9 and Figures 16–18 present the performance metrics and confusion matrices of RF and AB-RT considering the first five natural frequency shifts and the slope shifts of the corresponding mode shape for the delamination detection of cross-ply, angle-ply, and quasi-isotropic cantilever plate structures.

It is seen from Tables 7–9 that RF and AB-RT accurately localize the delamination. The high values (> 0.9) of F-Measure, AUC, and Kappa values indicate that these bagging and boosting techniques are robust and adaptive to detect delamination no matter which fiber orientation has been considered. The inclusion of the slope shifts of the mode shapes has increased the accuracy of the localization of delamination in y-axis regions of the cross-ply composite plate. Therefore, it can be concluded that considering slope shifts of the mode shapes eliminates the inaccurate prediction of the models caused by the symmetric differences in the natural frequency shifts. On the other hand, the addition of the slope shifts of the mode shapes has slightly affected the performance metrics of the

Table 8. The performance metrics of AB-RT and RF for delamination localization in the y-axis regions of the cross-ply, angle-ply, and quasi-isotropic composite plates considering both the natural frequency shifts and slope shifts.

Cross-ply				Angle-ply				Quasi-isotropic			
AB-RT				**AB-RT**				**AB-RT**			
Acc	***F-M***	***AUC***	κ	***Acc***	***F-M***	**AUC**	κ	***Acc***	***F-M***	***AUC***	κ
95.13%	0.951	0.973	0.946	93.50%	0.935	0.964	0.928	95.00%	0.950	0.972	0.944
RF				**RF**				**RF**			
Acc	***F-M***	***AUC***	κ	***Acc***	***F-M***	**AUC**	κ	***Acc***	***F-M***	***AUC***	κ
95.50%	0.955	0.996	0.950	93.50%	0.935	0.987	0.928	94.25%	0.942	0.992	0.936

Table 9. The performance metrics of AB-RT and RF for delamination localization in the interfaces regions of the cross-ply, angle-ply, and quasi-isotropic composite plates considering both the natural frequency shifts and slope shifts.

Cross-ply				Angle-ply				Quasi-isotropic			
AB-RT				**AB-RT**				**AB-RT**			
Acc	***F-M***	***AUC***	κ	***Acc***	***F-M***	**AUC**	κ	***Acc***	***F-M***	***AUC***	κ
100%	1.000	1.000	1.000	96.75%	0.968	0.982	0.964	98.50%	0.985	0.992	0.983
RF				**RF**				**RF**			
Acc	***F-M***	***AUC***	κ	***Acc***	***F-M***	**AUC**	κ	***Acc***	***F-M***	***AUC***	κ
100%	1.000	1.000	1.000	97.50%	0.975	1.000	0.972	99.25%	0.992	1.000	0.992

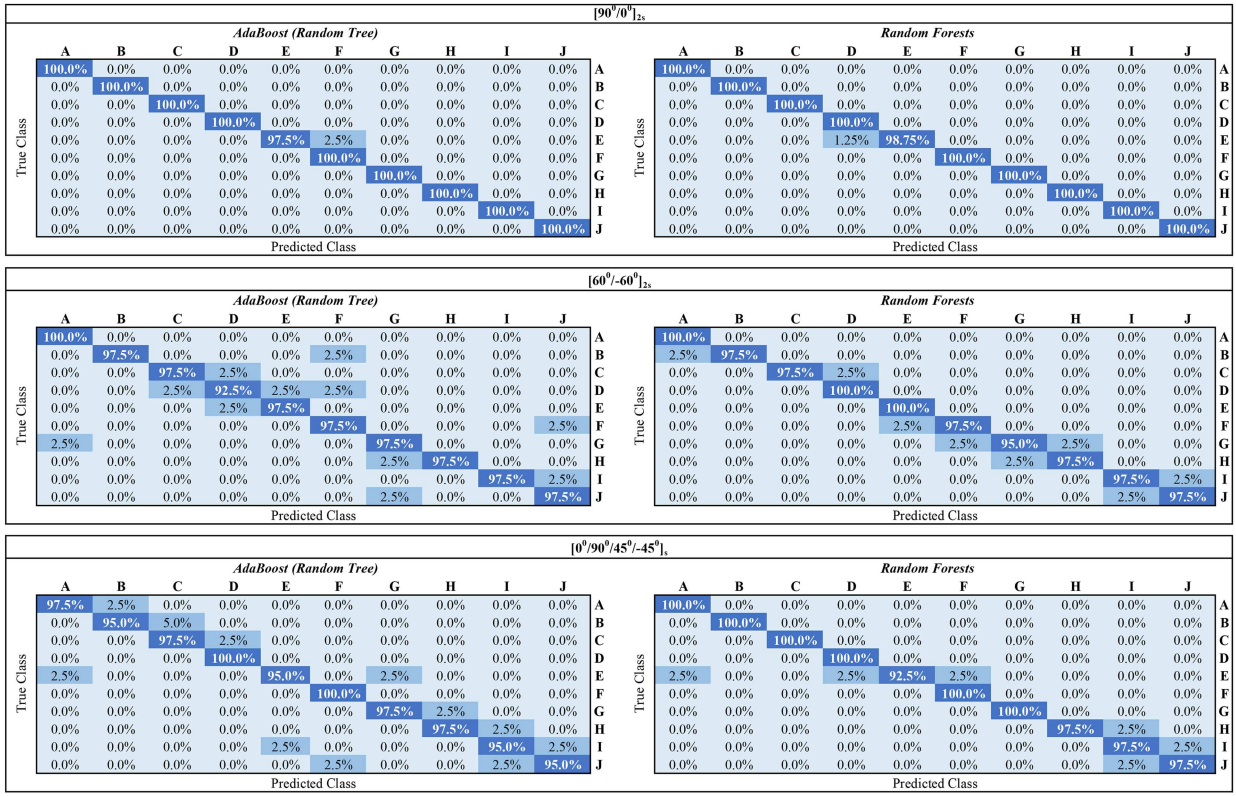

Figure 16. The confusion matrix of AB-RT and RF for delamination detection in x-regions considering both the natural frequency shifts and mode shape slope shifts.

Ensemble Learning techniques when localizing the delamination in x-axis regions and interfaces of the cross-ply plates. Similarly, the performance metrics of the models when localizing the delamination in x-axis regions, y-axis regions, and interfaces of the angle-ply and quasi-isotropic composite plates have been slightly increased when including the slope shifts of the mode shapes as input variables.

The confusion matrices given in Figures 16–18 indicate that no matter which input values have been

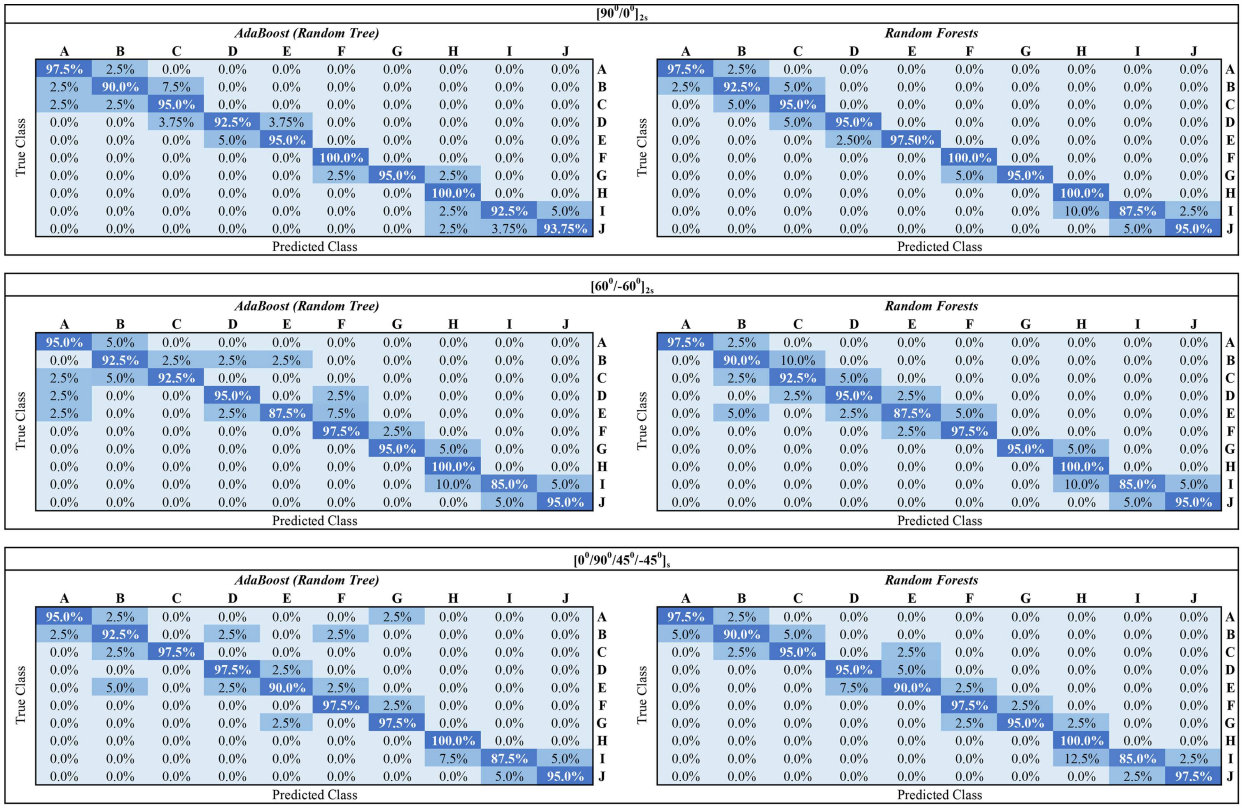

Figure 17. The confusion matrix of AB-RT and RF for delamination detection in y-regions considering both the natural frequency shifts and mode shape slope shifts.

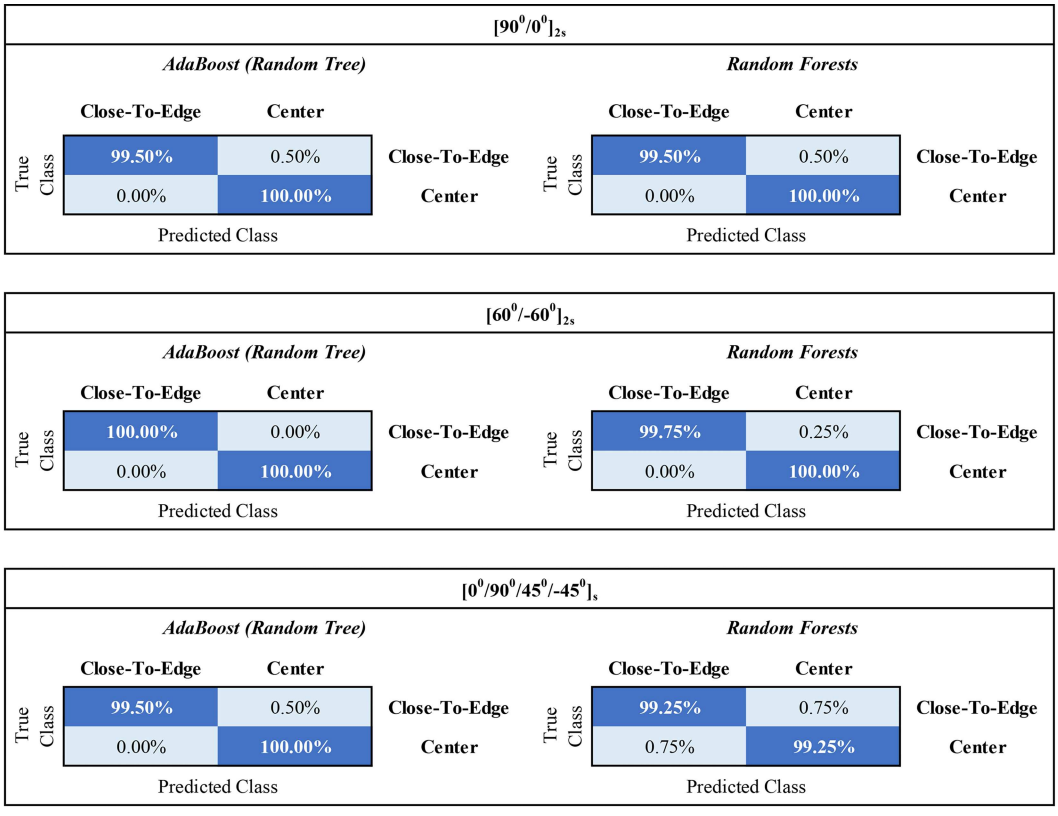

Figure 18. The confusion matrix of AB-RT and RF for delamination detection in interfaces considering both the natural frequency shifts and mode shape slope shifts.

chosen, the instances have successfully classified with high accuracy, except for the model built to predict the delamination location in the y-axis region of cross-ply composite using the first five natural frequency shifts only. According to Tables 4–6, for angle-ply and quasi-isotropic structures, the average localization (x-axis regions, y-axis regions, and interface) accuracy has been measured for RF and AB-RT as 93.67% and 93.39% respectively when only the natural frequency shifts have been considered. On the other hand, according to the results given in Tables 7–9, when both the natural frequency shifts and slope shifts of the corresponding mode shapes have been considered as input variables, the average accuracy values of the RF and AB-RT have increased to 97.64% and 97.49% respectively. Since the AUC, F-Measure, and Kappa values are higher than 0.9, it is concluded that these models are not only highly accurate but also robust and precise. The overall best accuracy has been obtained for cross-ply (98.38%), followed by quasi-isotropic (97.42%), and angle-ply plates (97.13%).

Considering the cross-ply structure and the given boundary conditions, the bagging and boosting models do not require slope shifts of the mode shapes for identifying the delamination location through the x-axis and the layers of the structure. However, the slope shifts may be required to train the bagging and boosting models for identifying delaminations in the x-axis if the constraint parameters of the cross-ply structure change. The remained structures having angle-ply and quasi-isotropic fiber orientations do not essentially require slope shifts of the mode shapes since the delamination detection accuracy values of bagging and boosting techniques are above 93.00%. Moreover, the additional consideration of the slope shifts of the mode shapes causes a slight increase in the delamination detection accuracy for those fiber orientations. Regarding the overall detection accuracy of the delamination in the y-axis of the composite plate, RF and AB-RT give close values that are 94.42% and 94.54% when they are trained with both natural frequency shifts and slope shifts of the mode shapes. The detection accuracy values of RF and AB-RT in the x-axis of the structure slightly decrease when slope shifts of the mode shapes are also considered. Therefore, regarding the models trained by only the natural frequency shifts, the average detection accuracy values of the delamination in the x-axis of the structure are 99.70% for RF and 99.92% for AB-RT. Layer-wise delamination detection results indicate that including slope shifts decrease the accuracy values just as it does for detecting delamination in the x-axis of the structure. Therefore, considering the models trained by only the first five natural frequency shifts indicate that the average detection accuracy values are 99.79% for RF and 99.92% for AB-RT. Considering the identification of the delamination considering its layer-wise position and the locations in the x- and y-axis, RF detects the delamination with an average accuracy of 97.97% while AB-RT detects the delamination with that 98.13%. Therefore, it can be concluded that AB-RT is slightly superior to RF in identifying delaminations of cross-ply, angle-ply, and quasi-isotropic cantilever composite plates.

5. Conclusions

In this study, delamination localization in cross-ply, angle-ply, and quasi-isotropic cantilever composite plates has been performed using Bagging (RF) and Boosting (AB-RT). The selection of input variables based on fiber orientation has been examined. Besides, the effects of the fiber orientation on the performance metrics of the Bagging and Boosting techniques have been measured. According to the results given in the previous section, the following conclusions have been drawn:

- Employing the natural frequency shifts and slope shifts of the corresponding mode shapes as input variables gives better results than considering only the natural frequency shifts for delamination localization. Besides, considering only natural frequency shifts may cause the machine learning model to make inaccurate localizations for cross-ply structures;
- Although the fiber orientation has affected the performance metrics of the Bagging and Boosting techniques, the minimum localization accuracy has been evaluated for the angle-ply plate as 97.13%. Therefore, the Ensemble Learning techniques are robust against the differences in fiber orientation;
- It is seen that the AB-RT localizes delamination with an average accuracy of 98.12% while it is 97.97% for RF. Regarding the fiber orientations, the best overall localization performance is evaluated for the cross-ply plate (98.38%), followed by quasi-isotropic (97.42%), and angle-ply plates (97.13%);
- The analysis results indicate that the Ensemble Learning techniques can be used as a powerful tool for structural health monitoring purposes. The performance metrics indicate that these models are robust and precise for delamination localization. Therefore, these techniques are strong candidates to be implemented in experimental cases.

References

1. Wisnom, M.R. "The role of delamination in failure of fibre-reinforced composites", *Philos. Trans. Royal Soc.*, **370**, pp. 1850–1870 (2012). DOI: 10.1098/rsta.2011.0441

2. Figueiredo, E., Park, G., Farraf, C.R., et al. "Machine learning algorithms for damage detection under operational and environmental variability", *Struct. Health Monitor*, **10**(6), pp. 559–572 (2011). DOI: 10.1177/1475921710388971

3. Chalouhi, E.K., Gonzalez I., Gentile, C., et al. "Damage detection in railway bridges using Machine Learning: application to a historic structure", *Procedia Eng.*, **199**, pp. 1931–1936 (2017). DOI: 10.1016/j.proeng.2017.09.287

4. Soo Loon Wah, W., Chen, Y.T., and Owen, J.S. "A regression-based damage detection method for structures subjected to changing environmental and operational conditions", *Eng. Struct.*, **228**, p. 111462 (2021). DOI: 10.1016/j.engstruct.2020.111462

5. Mirzabeigy, A. and Madoliat, R. "Damage detection in a double-beam system using proper orthogonal decomposition and teaching-learning based algorithm", *Sci. Iran.*, **27**(2), pp. 757–771 (2020). DOI: 10.24200/sci.2019.50520.1738

6. Jena, S.P. and Parhi, D.R. "Fault detection in cracked structures under moving load through a recurrent-neural-networks-based approach", *Sci. Iran.*, **27**(4), pp. 1886–1896 (2020). DOI: 10.24200/sci.2019.50363.1657

7. Saeed, R.A., Galybin, A.N., and Popov, V. "Crack identification in curvilinear beams by using Ann and ANFIS based on natural frequencies and frequency response functions", *Neural Compt. and Appl.*, **21**(7), pp. 1629–1645 (2011).
DOI: 10.1007/s00521-011-0716-1

8. Hakim, S.J.S. and Razak, A. "Structural damage detection of steel bridge girder using artificial neural networks and finite element models", *Compos. Struct.*, **14**, pp. 367–377 (2013). DOI: 10.12989/scs.2013.14.4.367

9. Paulraj, M., Yaacob, S., Majid, M.A., et al. "Structural steel plate damage detection using non destructive testing, frame energy based statistical features and artificial neural networks", *Procedia Eng.*, **53**, pp. 376–386 (2013). DOI: 10.1016/j.proeng.2013.02.049

10. Yan, B., Cui, Y., Zhang, L., et al. "Beam structure damage identification based on BP neural network and support vector machine", *Math. Probl. Eng.*, **2014**, pp. 1–8 (2014). DOI: 10.1155/2014/850141

11. De Fenza, A., Sorrentino, A., and Vitiello, P. "Application of artificial neural networks and probability methods for damage detection using lamb waves", *Compos. Struct.*, **133**, pp. 390–403 (2015). DOI: 10.1016/j.compstruct.2015.07.089

12. Satpal, S.B., Guha, A., and Banerjee, S. "Damage identification in aluminum beams using support vector machine: Numerical and experimental studies", *Struct. Cont. Health Monitor.*, **23**(3), pp. 446–457 (2015). DOI: 10.1002/stc.1773

13. Ghiasi, R., Torkzadeh, P., and Noori, M. "A machine-learning approach for structural damage detection using least square support vector machine based on a new combinational kernel function", *Struct. Health Monitor.*, **15**, pp. 302–316 (2016). DOI: 10.1177/1475921716639587

14. Neves, A.C., González, I., Leander, J., et al. "Structural health monitoring of bridges: A model-free ANN-BASED approach to damage detection", *J. Civil Struct. Health Monitor.*, **7**(5), pp. 689–702 (2017). DOI: 10.1007/s13349-017-0252-5

15. Kourehli S.S. and Karoumi, R. "Application of extreme learning machine to damage detection of plate-like structures", *Int. J. Struct. Stab. Dyn.*, **17**(7), 1750068 (2017). DOI: 10.1142/S0219455417500687

16. Ghiasi, R., Ghasemi, M.R., and Noori, M. "Comparative studies of metamodeling and ai-based techniques in damage detection of structures", *Adv. Eng. Softw.*, **125**, pp. 101–112 (2018). DOI: 10.1016/j.advengsoft.2018.02.006

17. Kourehli, S.S. "Prediction of unmeasured mode shapes and structural damage detection using least squares support vector machine", *Struct. Monitor. Maint.*, **5**(3), pp. 379–390 (2018). DOI: 10.12989/smm.2018.5.3.379

18. Khan, A. and Kim, H.S. "Assessment of delaminated smart composite laminates via system identification and supervised learning", *Compos. Struct.*, **206**, pp. 354–362 (2018). DOI: 10.1016/j.compstruct.2018.08.014

19. Jac Fredo, A., Abilash, R., Femi, R., et al. "Classification of damages in composite images Using Zernike moments and support vector machines", *Compo. B. Eng.*, **168**, pp. 77–86 (2019). DOI: 10.1016/j.compositesb.2018.12.064

20. Inkoom, S., Sobanjo, J., Barbu, A., et al. "Pavement crack rating using machine learning frameworks: Partitioning, Bootstrap Forest, boosted Trees, Naïve Bayes, and K-nearest neighbors", *J. Transp. Eng. B: Pavements* , **145**(3), 04019031 (2019).

21. Gomes, G.F., de Almeida, F.A., Junqueira, D.M., et al. "Optimized damage identification in CFRP plates by reduced mode shapes and GA-ANN methods", *Eng. Struct.*, **181**, pp. 111–123 (2019). DOI: 10.1016/j.engstruct.2018.11.081

22. Zhang, Z., Pan, J., Luo, W., et al. "Vibration-based delamination detection in curved composite plates", *Compos. -A. Appl. Sci. Manuf.*, **119**, pp. 261–274 (2019). DOI: 10.1016/j.compositesa.2019.02.002

23. He, M., Wang, Y., Ramakrishnan, K.R., et al. "A comparison of machine learning algorithms for assessment of delamination in fiber-reinforced polymer composite beams", *Struct. Health Monitor.*, **20**(4), pp. 1997–2012 (2021). DOI: 10.1177/1475921720967157

24. Jacobs, E.W., Yang, C., Demir, K.G., et al. "Vibrational detection of delamination in composites using a combined finite element analysis and machine learning approach", *J. Appl. Phys.*, **128**(12), 125104 (2020). DOI: 10.1063/5.0015648

25. Gillespie, D.I., Hamilton, A.W., Atkinson, R.C., et al. "Composite laminate delamination detection using transient thermal conduction profiles and machine elarning based data analysis", *Sensors*, **20**(24), p. 7227 (2020). DOI: 10.3390/s20247227

26. Jaanuska, L. and Hein, H. "Delamination quantification by haar wavelets and machine learning", *Mech. Compos. Mater.*, **58**, pp. 249–260 (2022).

27. Li, Y., Zhou, K., Qin, H., et al. "Machine learning approach for delamination detection with feature missing and noise polluted vibration characteristics", *Compos. Struct.*, **287**, 115335 (2022). DOI: 10.1016/j.compstruct.2022.115335

28. Reis, P.A., Iwasaki, K.M.K., Voltz, L.R., et al. "Damage detection of composite beams using vibration response and artificial neural networks", *Proc. Inst. Mech. Eng. L: J. Mater.: Des. Appl.*, **236**(7), pp. 1419–1430 (2021). DOI: 10.1177/14644207211041326

29. Mardanshahi, A., Shokrieh, M., and Kazemirad, S. "Identification of matrix cracking in cross-ply laminated composites using Lamb wave propagation", *Compos. Struct.*, **235**, 111790 (2020). DOI: 10.1016/j.compstruct.2019.111790

30. Zheng, T.Z., Tong, H., and Liang, X. "A two-step method for delamination detection in composite laminates using experience-based learning algorithm", *Struct. Health Monitor.*, **21**(3), pp. 965–983 (2021). DOI: 10.1177/14759217211018114

31. Moorthy, V. and Marappan, K. "Identification of delamination severity in a tapered FRP composite plate", *Compos. Struct.*, **299**, p. 116054 (2022). DOI: 10.1016/j.compstruct.2022.116054

32. Xu, Y., Zhou, H., Cui, Y., et al. "Full scale promoted convolution neural network for intelligent terahertz 3D characterization of GFRP delamination", *Compos. B: Eng.*, **242**, p. 110022 (2022). DOI: 10.1016/j.compositesb.2022.110022

33. Rautela, M., Senthilnath, J., Monaco, E., et al. "Delamination prediction in composite panels using unsupervised-feature learning methods with wavelet-enhanced guided wave representations", *Compos. Struct*, **291**, p. 115579 (2022). DOI: 10.1016/j.compstruct.2022.115579

34. Mardanshahi, A., Nasir, V., Kazemirad, S., et al. "Detection and classification of matrix cracking in laminated composites using guided wave propagation and artificial neural networks", *Compos. Struct.*, **246**, p. 112403 (2020). DOI: 10.1016/j.compstruct.2020.112403

35. Barman, S.K., Maiti, D.K., and Maity, D. "Vibration-based delamination detection in composite structures employing mixed unified particle swarm optimization", *AIAA J.*, **59**(1), pp. 386–399 (2021). DOI: 10.2514/1.J059176

36. Lim, D.K., Mustapha, K., and Pagwiwoko, C. "Delamination detection in composite plates using random forests", *Compos. Struct.*, **278**, p. 114676 (2021). DOI: 10.1016/j.compstruct.2021.114676

37. Petyt, M. *Introduction to Finite Element Vibration Analysis*, Cambridge University Press (2010).

38. Ganesh, S., Kumar, K.S., and Mahato, P. "Free vibration analysis of delaminated composite plates using finite element method", *Procedia Eng.*, **114**, pp. 1067–1075 (2016). DOI: 10.1016/j.proeng.2016.05.061

39. Farsadi, T., Şener, O., and Kayran, A. "Free vibration analysis of uniform and asymmetric composite pretwisted rotating thin walled beam", *Proc. of the ASME 2017 Int. Mech. Eng. Congr. and Expos*, **1**, V001T03A016 (2017). DOI: 10.1115/IMECE2017-70531

40. Breiman, L. "Random forests", *Mach. Learn.*, **45**, pp. 5–32 (2001).

41. Freund, Y. and Schapire, R. "A decision-theoretic generalization of on-line learning and an application to boosting", *J. Comput. Syst. Sci.*, **55**(1), pp. 119–139 (1997). DOI: 10.1006/jcss.1997.1504

Biographies

Oguzhan DAS is an Assistant Professor at the National Defence University, Air NCO Higher Vocational School, Department of Aeronautics Sciences, Turkey. He completed his PhD in the field of Machine Theory and Dynamics regarding structural dynamics of composite and metallic structures at Dokuz Eylül University, Department of Mechanical Engineering, Turkey. He published numerous studies in SCI-E, ESCI, and SCOPUS-indexed journals related to structural health monitoring, fault diagnosis of machines, composite characterization, structural vibration, buckling, and dynamic stability. His research interests are intelligent fault diagnosis and prognosis methods for structures and machines, dynamics of damaged structures, finite element method, and composite structures.

Duygu Bagci DAS is a Lecturer in the computer programming department at Ege University, Turkey. She completed her PhD on artificial intelligence-based human activity recognition in the Computer Engineering Department at Dokuz Eylül University, Türkiye. She has several publications indexed in SCI-E, ESCI, and SCOPUS related to intelligent fault diagnosis of machines, human activity recognition, and intelligent biomedical systems. Her research interests are in sensor-based intelligent systems in the field of engineering, computer science, and healthcare.